ELSEVIER

Journal of Hazardous Materials 49 (1996) 29–47

JOURNAL OF HAZARDOUS MATERIALS

A model of the motion and dilution of a heavy gas cloud released on a uniform slope in calm conditions

G.A. Tickle

AEA Technology Thomson House, Risley, Warrington, Cheshire WA3 6AT UK

Received 20 October 1994; accepted 15 November 1995

Abstract

A model of the motion of a heavy gas cloud down a uniform slope in calm ambient conditions is extended to include a model for the dilution of the cloud. The dilution is modelled assuming that entrainment is based on the advection velocity. The model's main predictions appear to be broadly consistent with the experimental observations. Model parameters are an entrainment coefficient and a frontal Froude number, and values for these have been determined by fitting to the experimental data.

Keywords: Dilution; Heavy gas colud; Model; Motion

1. Introduction

Many hazardous substances (which may be stored in large quantities on industrial sites) can, if released into the environment, result in the formation of a heavy gas cloud. The dispersion of such a gas cloud is of significant practical interest, particularly in the assessment of possible hazards associated with industrial plant. Integral (or box) models are commonly used for predicting the dispersion of such hazardous clouds, and an understanding of the main influences on the dispersion needs to be built into such models.

One such feature is the influence of sloping ground on dense gas dispersion. The slope is expected to have a significant effect upon the initial motion of the cloud, by virtue of the resultant gravitational force component acting down the slope. Additionally, the presence of a slope might significantly influence the geometry and dilution rate of the cloud as compared with that over flat ground.

Currently published integral models for instantaneously released clouds ([1]; [2]) are generalisations of flat ground models and include models for the advection of the cloud

PII S0304-3894(96)01747-5

by applying a balance of gravitational and drag forces for the bulk cloud. An alternative advection model ([3]) has been suggested which involves the advection of a wedge shaped cloud down a slope, with the motion resulting from a balance of gravity and air resistance at the front. This wedge shaped model is appealing because it is based on a similarity solution of the shallow water equations, although the validity is questionable, as the solution is derived for the case of a non-entraining cloud.

The subject of this paper is the addition of an entrainment model to the wedge advection model of Webber et al. [3]. As we believe that it is desirable to understand first the influences on dispersion in isolation, we restrict discussion to that of dispersion in calm conditions where dilution is by virtue of the cloud's motion under gravity. The case of an isothermal cloud which conserves buoyancy will be considered, as this allows analytical solution of the model equations without recourse to numerical solution, yet (in principle) is readily generalisable to include non-isothermal clouds. Experimental data ([4,5]) will be used for comparison with the main predictions of the model and for determining possible values for empirical coefficients.

2. The model of Webber et al. [3]

Webber et al. [3] presented a model of the motion of a heavy gas cloud released instantaneously on a shallow uniform slope. In that work it was demonstrated that the shallow water equations for a non-entraining cloud on a slope, together with suitable boundary conditions, permit a shallow "wedge" shaped cloud to be formed. Webber's model of cloud motion on a slope is based on this similarity solution. The solution relies on a resistive force at the cloud front which balances the gravitational force, analogous to the frontal relationship for gravity slumping on flat ground. Only the advection velocity of the cloud was modelled. In comparisons with experimental data, air entrainment was not modelled, but estimated from concentration measurements.

Before discussing how we can extend the model to include air entrainment, it is useful to summarise the cloud geometry and the advection model of Webber et al., as these will also be applied to the entraining cloud model.

2.1. Cloud geometry

The geometry of the cloud is wedge shaped, with the cloud's lateral extent being predicted as π times the downslope extent and the top of the cloud horizontal. The cloud shape is shown schematically in Fig. 1. The cloud maintains the same shape and does not get wider as it moves down the slope: the frontal motion of the cloud is such that in the absence of entrainment the spreading results in bulk movement down the slope. As the cloud geometry is fixed there is only one length scale for the cloud; we take this to be Λ, the horizontal extent in the down-slope direction. The gradient Γ of the slope is defined to be the tangent of the angle that the slope makes with the horizontal. For simplicity we refer to Γ simply as the slope. The maximum height of the front edge of the cloud is $H = \Gamma\Lambda$.

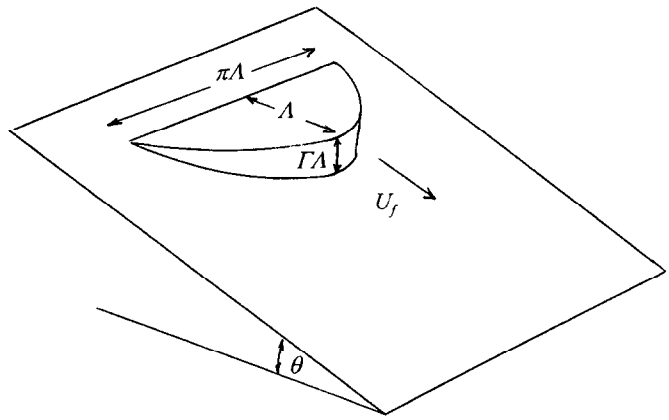

$\Gamma = tan\ \theta$

Fig. 1. Geometry of the wedge shaped shallow water similarity solution (from [3]).

Many geometric quantities of the cloud are found to involve integral coefficients of the form

$$\Omega_n = \int_{-\pi/2}^{\pi/2} cos^n\omega \, d\omega \tag{1}$$

For example, the top and edge areas, denoted A_T and A_E respectively, are

$$A_T = 2\Omega_4 \Lambda^2$$

$$A_E = 2\Omega_3 \Gamma \Lambda^2 \tag{2}$$

and the volume V is given by

$$V = \Omega_6 \Gamma \Lambda^3 \tag{3}$$

The cloud centroid is located a horizontal distance $\xi\Lambda$ from the back edge of the cloud, where $\xi = 2\Omega_8/3\Omega_6 = 7/12$.

[The above integral values are easily determined, and are given below

$\Omega_3 = 4/3\ \Omega_4 = 3\pi/8\ \Omega_6 = 5\pi/16\ \Omega_8 = 35\pi/128$

The coefficients may be generated by using the relationship

$$\Omega_n = \frac{n-1}{n}\Omega_{n-2}$$

with $\Omega_0 = \pi$ and $\Omega_1 = 2$.]

2.2. Advection velocity

The front velocity U_f of the cloud down the slope is given in [3] by

$$U_f = K_f(g'\Gamma\Lambda)^{1/2} \tag{4}$$

where K_f is a Froude number for the resisted motion of the cloud edge, $g' = g(\rho - \rho_a)/\rho_a$ is the reduced gravitational acceleration of the cloud, and Γ and Λ are the slope and the cloud length scale as defined previously. For flat ground a value of $K_f \approx 1.07$ is found to optimise fits to the Thorney Island trials ([6]). Webber et al. [3] also used this value for their comparison of the advection model on a slope. In principle, given the different nature of the flow, a different value might be more appropriate. We return to discuss this later when we compare the entraining cloud model with data.

3. The air entrainment model

We now consider modelling the dilution of the cloud on a slope. The similarity solution of Webber et al. [3] is derived for a non-entraining cloud, and solution of the shallow water equations including entrainment directly is fairly difficult. Progress might be possible by assuming that the non-entraining similarity solution pertains even when entrainment occurs. This is not too dissimilar to the way integral models treat gravity spreading on flat ground. In this paper we shall pursue this approach, using an entrainment assumption to specify the rate of dilution of the cloud.

The velocity U_f is the only velocity scale available, and so (following Morton et al. [7]) on dimensional grounds we consider a model of entrainment of the form

$$\frac{d}{dt}(\rho V) = \alpha_\Gamma \rho_a A U_f \tag{5}$$

where A is the characteristic area associated with the mass transfer process and α_Γ is a (dimensionless) entrainment coefficient. We discuss below some possible choices for A and α_Γ.

3.1. Choice of entrainment coefficient

Ultimately the entrainment coefficient must be determined from experimental measurements of actual flows. First, however, it is instructive to consider what dependences we might expect for this type of flow down a slope.

Firstly, we shall assume Reynolds number independence of the flow and hence the entrainment coefficient. This is expected to be well satisfied for most large scale releases in the field and to hold approximately for the experimental data with which we shall compare the model.

If the flow is not stably stratified then one might suppose that the entrainment coefficient will take a constant value as for vertical buoyant plumes (e.g. [7]). For stably stratified flow, the amount of entrainment will be reduced as compared with a non-stratified flow. Ellison and Turner [8] investigated two-dimensional dense plumes on slopes and found that the entrainment coefficient was dependent on a bulk Richardson number Ri defined by

$$Ri = \frac{g' h \cos\theta}{U^2} \tag{6}$$

where h is a measure of the depth of the plume layer, θ is the angle to the horizontal and U is the plume velocity down the slope. Ellison and Turner's measurements showed that the entrainment coefficient fell off rapidly with increasing Ri (and therefore with decreasing slope).

For the case we wish to consider here—that of the wedge shaped dense cloud moving down a slope—we can define a Richardson number based on the conditions at the cloud front (and on the centreline). The velocity U is assumed to be given by U_f in Eq. (4) and is hence related to $g'H$. In this case Ri is a function only of slope. In other words, the effect of density stratification appears only through a slope dependence to the entrainment coefficient. As in the case of the two-dimensional plumes studied by Ellison and Turner, we might expect the entrainment to decrease with decreasing slope.

3.2. Choice of the area A

As we are assuming that the geometry of the cloud is fixed, then the area A must be proportional to the square of the cloud length scale.

In principle we could have separate terms for "top" and "edge" areas, with different entrainment coefficients for each. This is usually the case for flat ground dense gas models which model "top" and "edge" entrainment separately. It can be shown, however, that for the assumed wedge geometry the two terms are proportional, and the constant of proportionality (which will be slope dependent) may be absorbed into a single entrainment coefficient. For our comparison with data we choose A to be the top area A_T, and note that we could equally well use the edge area A_E or some other measure of area. Of course we should add the qualification that different choices of A will give different entrainment coefficients and that when quoting an entrainment coefficient we need to specify which definition of A is appropriate.

4. Model equations for an isothermal cloud

The above equations for advection velocity and entrainment rate, together with a contaminant conservation equation and cloud geometry, specify the model for an isothermal wedge shaped cloud on a uniform slope. Generalisation to include non-isothermal clouds is, at least in principle, straightforward, following the same approach as flat ground box models.

We may write the equations as

$$\begin{aligned}
&\frac{dX_f}{dt} = U_f = K_f(g'\Gamma\Lambda)^{1/2}\\
&\frac{dV}{dt} = A_T\alpha_\Gamma U_f\\
&CV = C_0V_0\\
&V = \Omega_6\Gamma\Lambda^3\\
&A_T = 2\Omega_4\Lambda^2
\end{aligned} \tag{7}$$

Here, C represents the volumetric concentration of contaminant, and the subscript 0 represents the initial conditions; X_f represents the downslope distance of the cloud front.

In the above we have used buoyancy conservation (the buoyancy is given by $B_0 = g'V$, and is conserved for an isothermal cloud) to remove the density terms from Eq. (5).

4.1. Solutions of the model equations

Using buoyancy conservation we may solve Eq. (7).

The solutions are given here in terms of the cloud length Λ, non-dimensionalised by the value at an initial time $t = 0$ (here all values with subscript 0 refer to values at $t = 0$)

$$\zeta = \Lambda/\Lambda_0 = (\tau + 1)^{1/2} \tag{8}$$

with

$$\tau = t/T_0$$

$$T_0 = \left(\frac{3\Omega_6^{5/6}}{4\Omega_4}\right)\left(\frac{\Gamma^{1/3}}{\alpha_\Gamma K_f}\right)\left(\frac{V_0^{2/3}}{B_0^{1/2}}\right) \tag{9}$$

giving

$$A_T/A_{T0} = \zeta^2$$

$$V/V_0 = \zeta^3$$

$$C/C_0 = \zeta^{-3}$$

$$U_f/U_{f0} = \zeta^{-1}$$

$$\frac{X_f - X_{f0}}{2T_0U_{f0}} = (\zeta - 1) \tag{10}$$

4.2. Properties of the solutions

Immediately we can see from the above solution that for time $t \gg T_0$ the dependence on time is as follows

- the linear dimension Λ and frontal distance X_f increase as $t^{1/2}$,
- the top area A_T increases as t,
- the concentration C decreases as $t^{-3/2}$ and
- the velocity U_f down the slope decreases as $t^{-1/2}$.

It is also instructive to consider the explicit dependences in more detail, especially the dependence of the concentration and arrival time predictions upon the slope Γ, the entrainment coefficient α_Γ, and the Froude number K_f.

Firstly, the concentration at a given time t for $t \gg T_0$ is given by

$$\frac{C}{C_0} \to \left(\frac{3\Omega_6^{5/6}}{4\Omega_4}\right)^{3/2}\left(\frac{\Gamma^{1/2}}{(\alpha_\Gamma K_f)^{3/2}}\right)\left(\frac{V_0}{B_0^{3/4}}\right)t^{-3/2} \tag{11}$$

The dependence on V_0 and B_0 and t follows from dimensional considerations. If there were no slope dependence to the product $\alpha_\Gamma K_f$, then the influence of increasing slope would be to lead to a higher concentration at a given time.

We can also consider the dependence of concentration on front position X_f, when $X_f \gg 2T_0U_{f0}$ and $X_f \gg X_{f0}$. This is given by

$$\frac{C}{C_0} \to \left(\frac{3\Omega_6^{2/3}}{2\Omega_4}\right)^3 \frac{\Gamma^2}{\alpha_\Gamma^3} V_0 X_f^{-3} \tag{12}$$

We note that at a fixed X_f, C/C_0 is independent of both the Froude number and the buoyancy B_0. The influence of the slope for a fixed entrainment coefficient is to increase the concentration for larger slopes. The concentration at a given distance also depends fairly strongly (as the cube) on the value of the entrainment coefficient. The dependence on volume is as expected from dimensional analysis.

Also of interest is how the cloud arrival time varies at a given position X_f (again when $X_f \gg 2T_0U_{f0}$ and $X_f \gg X_{f0}$). We find in this case that the arrival time varies as

$$t \to \left(\frac{\Omega_4}{3\Omega_6^{1/2}}\right)\left(\Gamma^{-1/3}\frac{\alpha_\Gamma}{K_f}\right) B_0^{-1/2} X_f^2 \tag{13}$$

which depends on the ratio of the entrainment coefficient and the Froude number in addition to the slope. We note that for a fixed buoyancy the arrival time is independent of the volume of the release. Neglecting any possible slope dependence to α_Γ/K_f, then the Γ dependence would be fairly weak by virtue of the one third power.

5. Comparison with experiment

Comparison with experiment is essential both for verifying the model and for determining the model's empirical coefficients. Here we give details of a comparison of the model with data and of the values determined for the empirical coefficients.

5.1. The experiments of Schatzmann et al. [4]

Schatzmann and co-workers used a boundary layer wind tunnel to model the instantaneous release of a dense gas on an inclined plane in conditions of zero ambient flow. Further details of the experimental setup are given in refs. [3] and [4]. A 450 cm^3 cylinder of SF_6–air mixture was instantaneously released on a slope in zero ambient flow. Each release was repeated five times using identical initial conditions with zero ambient wind. Three different slopes ranging from 4% to 11.63% were used.

In this study, in addition to the centreline arrival times which were determined previously ([3]), we have also analysed data from sensors which were placed off-axis—this gives information about the lateral extent of the cloud (and also, potentially, information on cloud concentration profiles).

5.2. Data analysis and interpretation

5.2.1. Assumptions

Given the limited available experimental data and the implicit assumptions in the wedge model, we make the following assumptions regarding analysis and interpretation of the data

(a) Peak concentrations as measured by sensors are taken to correspond to the cloud average values as predicted by the model.

(b) The arrival time at a sensor is taken to be the time when the peak concentration occurs.

(c) Comparisons are made with the mean values of the five repeats for each slope. Estimates of errors are obtained from the standard deviation over these repeats.

(d) There are no air currents present which affect the cloud, other than those induced by the cloud's motion down the slope.

(e) The cloud is released effectively instantaneously.

Concentrations (and arrival times) obtained in this way will be sensitive to the measuring instrument (and its averaging time). However, in our opinion, a more sophisticated treatment is unwarranted for this study, as it would require making further assumptions regarding the motion and dilution of the cloud.

If the cloud concentration profiles are self-similar, then (at least for centreline values) the influence of a non-uniform profile may be absorbed into the empirically determined coefficients α_Γ and K_f.

The release mechanism of Schatzmann means that (c) is likely to be well approximated, although the time taken for the flow to develop from the initial cylindrical shape to that for the cloud moving down the slope may need to be considered. We discuss this later.

5.3. Dilution of the cloud

5.3.1. C/C_0 against time

Fig. 2(a) shows how the concentration falls off with arrival time at the various on-axis sensors. The data appear to indicate a steeper fall off in time for steeper slopes. Also shown in Fig. 2(a) are the model predictions using a single constant value of $\alpha_\Gamma K_f$ fitted for all the slopes. As discussed earlier, the model asymptotically shows a $t^{-3/2}$ behaviour which is somewhat steeper than $t^{-\alpha_E}$ behaviour which would be obtained for slumping on flat ground with an edge entrainment coefficient of $\alpha_E \sim 0.7$ (which is generally accepted to optimise fits to field trials, e.g. [6]). Judging from the slope of Schatzmann's data, it appears to indicate a more rapid dilution than would be obtained for a slumping cylinder on flat ground, although perhaps not as rapid as predicted by the wedge model.

Also evident in Fig. 2(a) is the fact that assuming a constant $\alpha_\Gamma K_f$ for all slopes leads to the model predicting greater dilution for shallower slopes, whereas Schatzmann's data appear to indicate the converse. This would seem to imply that we should allow $\alpha_\Gamma K_f$ to increase with increasing slope, as perhaps would be expected from the discussion on the expected behaviour of the entrainment coefficient.

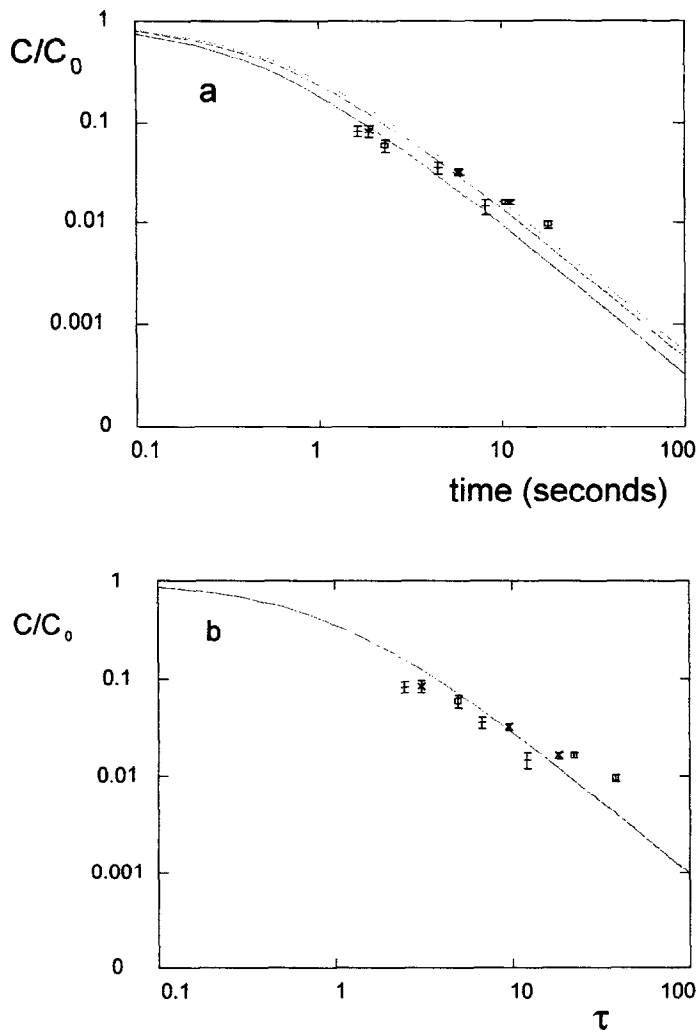

Fig. 2. (a) Volumetric concentration (normalised to 1 at the source) as a function of time. Schatzmann's data compared with the model for various slopes. The model predictions are with constant entrainment coefficient and Froude number for all slopes. Error bars are standard deviations over five repeats. □, solid line, 4%; x, dashed line, 8.6%; +, dotted line, 11.63%. (b) Volumetric concentration (normalised to 1 at the source) as a function of non-dimensional time. Schatzmann's data (□, 4%; x, 8.6%; +, 11.63%) compared with the model (solid line) which has an asymptotic $\tau^{-3/2}$ dependence at large τ. Error bars are standard deviations over five repeats.

Fig. 2(b) shows the same data plotted in non-dimensional form. Here the wedge model predictions for all slopes are represented by a single line and the fitted $\alpha_\Gamma K_f$ value determines the scatter of data points about this line. For a perfect fit the data would also collapse to the line.

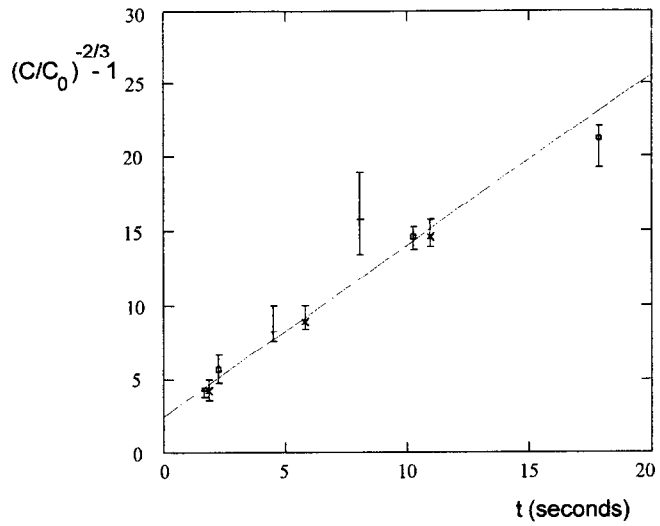

Fig. 3. $(C/C_0)^{2/3} - 1$ as a function of time from Schatzmann's data (□, 4%; x, 8.6%; +, 11.63%). The solid line represents the best overall fit for all slopes. Error bars are standard deviations over five repeats.

5.3.2. $(C/C_0)^{-2/3} - 1$ against time

As an alternative means of viewing the time dependence of the dilution, Fig. 3 shows a graph of $(C/C_0)^{-2/3} - 1$ against arrival time. If the time dependence from time $t = 0$ is as predicted by the wedge model, then a graph of $(C/C_0)^{-2/3} - 1$ against time should be a straight line for each Γ, each of which should pass through the origin.

In that the data for each Γ fall approximately on a straight line, the data appear to be consistent with the predicted time dependence. We find that a single line can be fitted to agree reasonably well with the data for *all* the slopes. The best fit single line for all the slopes has $T_0 = 0.87$ s; this is the line shown in Fig. 3. This implies that a single T_0 value can adequately represent the data within the estimated errors, implying a $\Gamma^{1/3}$ dependence of $\alpha_\Gamma K_f$. However, as mentioned earlier, it may appear that steeper slopes lead to more rapid dilution and hence have smaller T_0.

It is clear that the best fit (minimising the χ^2 statistic) straight lines do not pass through the origin (intercept values on the C/C_0 axis for fits to each slope are given in Table 1). This is to be expected because the initial release geometry is a cylinder and it seems reasonable to allow a finite time to develop into a wedge shape. We shall return to discuss this later.

Table 1
Fitted time scales for the concentration–time data for each slope and for the combined fit for all slopes

Slope (%)	Time scale T_0 (s)	Intercept concentrationratio C_i/C_0
4	0.98	0.10
8.6	0.88	0.17
11.6	0.62	0.23
All	0.87	0.15

5.4. Advection of the cloud

5.4.1. Arrival time as a function of distance

Fig. 4(a) illustrates the on-axis cloud arrival times as a function of distance for each slope. The lines on Fig. 4(a) illustrate the model prediction using the constant $\alpha_\Gamma K_f$ from the fit to the concentration data for all slopes (described above) and a value of K_f to optimise the fit (for all slopes) to the advection data. The model's capability for

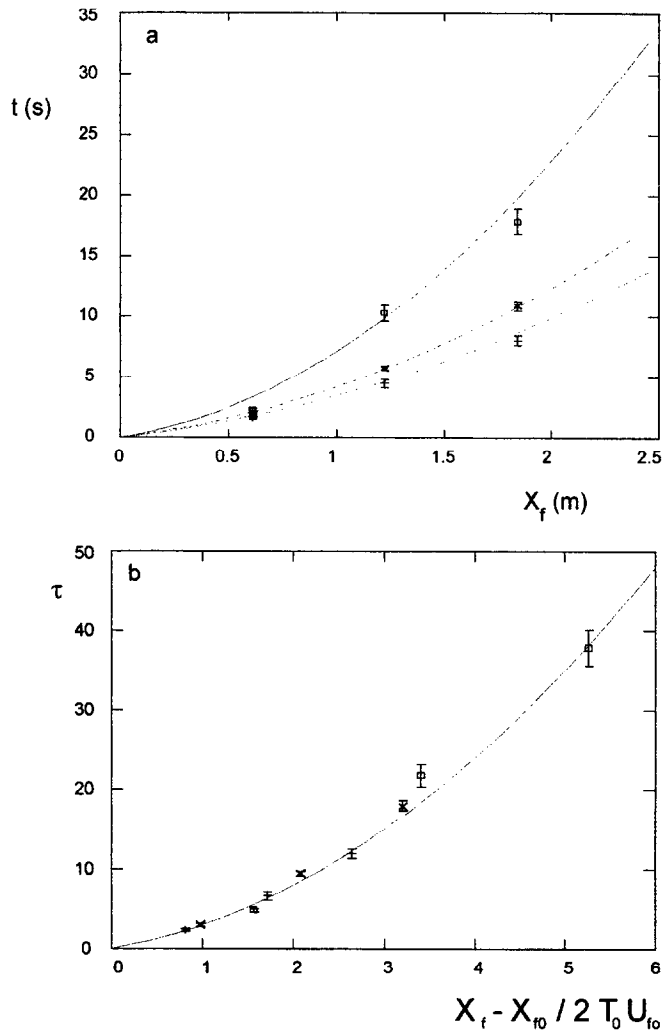

Fig. 4. (a) Centreline cloud arrival time as a function of distance. Schatzmann's data compared with model predictions assuming constant entrainment α_Γ and Froude number K_f for all slopes (□, solid line, 4%; x, dashed line, 8.6%; +, dotted line, 11.63%). Error bars are standard deviations over five repeats. (b) Non-dimensionalised cloud centreline arrival time as a function of non-dimensional distance. The model predictions collapse to a single line.

Table 2
Fitted values of entrainment coefficient and Froude number to the concentration and arrival time data. Fits are from time $t = 0$

Slope	Entrainment coefficient	Frontal Froude number
All	0.034	0.59
0.04	0.026	0.56
0.086	0.035	0.54
0.1163	0.045	0.67

representing the slope dependence of the advection of the cloud front is impressive given that only a single parameter (K_f) has been fitted.

With the Froude number K_f determined, the entrainment coefficient α_Γ follows from $\alpha_\Gamma K_f/K_f$. Table 2 gives the values determined for the entrainment coefficient and Froude number obtained by fitting to all slopes (as described above) and to each slope individually. Overall, an entrainment coefficient of 0.034 and a Froude number of 0.59 are found to be optimum (to minimize the χ^2 statistic). If each slope is fitted individually, then the model gives closer agreement with the data (particularly for the dilution of the cloud) largely by virtue of fitting a smaller number of points using more parameters. The results from these individual fits appear to indicate an entrainment coefficient increasing with increasing slope and a Froude number which remains fairly constant, although because of the limited available data we are unable to state whether this trend is statistically significant. Note that all the above results idealise the wedge model as applying from $t = 0$, with no initial dilution.

An alternative view is shown in Fig. 4(b), which has been non-dimensionalised such that the data for all slopes should collapse onto one curve.

Table 3 shows a comparison of the predicted and observed arrival times at each of the sensors.

Table 3
Mean arrival times from Schatzmann's data compared with model predictions

Sensor position (mm)	Arrival time (s)					
	4% slope		8.6% slope		11.63% slope	
	experiment	model	experiment	model	experiment	model
(61,30, 0.00)	2.3(1)	2.65	1.86(8)	1.79	1.65(6)	1.54
61.30,22.91)	–	2.76	–	1.87	1.88(4)	1.63
(61.30,45.98)	3.9(2)	3.09	3.3(1)	2.19	2.8(1)	1.98
(61.30,76.63)	10.0(3)	3.96	9.3(5)	–	–	–
(122.61,0.00)	10.3(7)	8.80	5.8(2)	5.24	4.5(3)	4.34
(122.61,22.91)	–	8.93	–	5.35	4.8(2)	4.45
(122.61,76.63)	18.4(7)	10.28	12.8(4)	6.74	–	6.06
(183.91,0.00)	17.8(10)	18.20	10.9(4)	10.21	8.0(4)	8.26
(183.91,38.32)	22.4(18)	18.59	12.5(6)	10.57	10.2(7)	8.61

Mean arrival time from Schatzmann's data for both on- and off-axis sensors. The bracketed numbers indicate the standard deviations over the five repeats. A dash (–) indicates that no value is available for that sensor position. The model predictions are those with constant $\alpha_\Gamma = 0.034$ and $K_f = 0.59$.

5.4.2. Advection velocity of the cloud

An alternative means of estimating the frontal Froude number is from the cloud frontal velocity; this is of necessity fairly indirect as velocity is not measured directly in Schatzmann's data and must be inferred from the arrival times at the sensors.

We estimate the front velocity U_f (by interpolation) at the arrival time at a given sensor, and from the concentration measurements we estimate the cloud volume V at this time. Hence the Froude number K_f follows from the relationship

$$U_f = K_f \Omega_6^{-1/6} \Gamma^{1/3} \left(\frac{B_0^{1/2}}{V^{1/3}} \right) \tag{14}$$

Table 4 shows the Froude number for each slope estimated in this way, together with the mean value for all slopes. This method of estimating Froude number has the advantage that it is independent of the entrainment model's ability to predict the cloud size correctly, as the concentration measurements rather than concentration predictions are used directly.

The Froude number determined in this way appears to be fairly constant over all the slopes with a mean value of 0.65—this is consistent with the value obtained from fitting to the arrival time–distance data as shown in Table 2.

5.5. Summary of the comparison of the model with data

5.5.1. Dilution of the cloud

Summarising the above results we find

- Steeper slopes appear to lead to more rapid (in time) dilution, although a single time scale for all slopes is also consistent with the data.
- The data are consistent with a $t^{-3/2}$ time dependence predicted by the wedge model for concentration.
- Initial dilution of the cloud is indicated which is not accounted for by the wedge model.
- Individual fits to each slope appear to indicate that $\alpha_\Gamma K_f$ increases more rapidly than $\Gamma^{1/3}$. This, together with the observation from the advection analysis that the Froude

Table 4
Estimated Froude number from velocity determination and concentration data

Slope	Position (m)	Velocity (m s^{-1})	Froude number
0.04	0.613	0.163	0.70
	1.226	0.079	0.52
0.086	0.613	0.230	0.69
	1.226	0.138	0.57
0.1163	0.613	0.279	0.75
	1.226	0.195	0.70
Mean			0.65

number appears approximately independent of slope, indicates that the entrainment coefficient of the model may increase with increasing slope, although this dependence appears fairly weak.
- The value of the entrainment coefficient (based on the top area of the cloud) is small compared with 1 (typically around 0.03).

5.5.2. Advection of the cloud

The main results are
- As expected, steeper slopes lead to a larger velocity for the front of the cloud.
- The data exhibits deceleration of the cloud frontal speed with distance.
- The position of the cloud front is consistent with the $t^{1/2}$ dependence predicted by the wedge model.
- A constant Froude number (of 0.59) fits the data well if one assumes a constant entrainment coefficient of 0.034 for all slopes.
- If the Froude number is allowed to vary with slope together with the entrainment coefficient, the best fit indicates that the Froude number increases with slope (from around 0.5 to 0.7 over the range of slopes considered), although the χ^2 values for the fits are not as good as assuming constant coefficients.

5.6. Cloud shape

The off-axis arrival times are given in Table 3, where they may be compared with the model predictions. The off-axis predictions are not as good as on-axis, particularly at large off-axis distances compared with the (expected) size of the cloud. In general the model predicts the cloud arrives off-axis too soon compared with the data. This implies that the cloud front may be more curved than predicted by the wedge model and that the trailing material moves at a lower velocity.

5.7. Formation of the wedge shaped cloud

As mentioned above, the data indicate that the wedge model is probably not consistent with the observed dilution from $t = 0$, although it may be consistent for dilution subsequent to a short initial phase. It would be useful if we could estimate the dilution and duration of this initial phase. From the data (see Fig. 3 and Table 1) it appears that the initial dilution and the dilution time decrease with increasing slope.

Consistent with this we have attempted to estimate the initial wedge conditions using the following approach.
- The spread and dilution of the cloud are modelled initially as a slumping cylinder on flat ground so long as the cloud height $H \gg \Gamma R$, where R is the radius of the cloud.
- When $H = \Gamma R$ we convert the cloud from a cylindrical shape to a wedge shape by conserving the cloud concentration and (arbitrarily) the cloud front position.

In this way we estimate the initial concentration and time for starting the wedge model. This will introduce a slope and an initial aspect ratio dependence to the volume V_0 in the above wedge equations and also the time delay t_0.

Applying a cylindrical box model with only edge entrainment, we find that the initial volume of the wedge solution becomes

$$V_0\left(\frac{\Gamma}{a_0}\right)^{-2\alpha_E/(3-2\alpha_E)} \tag{15}$$

where α_E is an edge entrainment coefficient and a_0 is the initial aspect ratio of the cylinder (defined as H_0/R_0).

The time delay t_0 is

$$t_0 = \gamma\left(\frac{V_0^{2/3}}{B_0^{1/2}}\right)$$

$$\gamma = \frac{1}{2K_{fc}}\pi^{-1/6}a_0^{-2/3}\left[\left(\frac{\Gamma}{a_0}\right)^{-2/(3-2\alpha_E)} - 1\right] \tag{16}$$

where K_{fc} is the Froude number for the cylindrical spreading (= 1.07 from Thorney Island trials [6]).

The effect of the above is that there will be more initial dilution for shallower slopes and a longer time delay before the wedge is assumed. For the 4% slope this model indicates an initial dilution to C/C_0 of approximately 0.06 and a time delay of the order of 1 s, whereas for the 11.63% slope we find an initial dilution of 0.15 and a time delay of 0.2 s. These figures are consistent with the observed initial dilutions as shown in Fig. 3.

Allowing for this initial dilution phase, we can repeat the fits for entrainment coefficient and Froude number. The resultant model coefficients are given in Table 5.

It can be seen that the effect of allowing for the initial dilution is to decrease the entrainment coefficient and to increase the Froude number. The enhanced initial dilution for the 4% slope shows the most marked effect—this is because the cloud must slump further before the backedge touches the ground. It can also be seen that the fitted Froude number shows greater variation and we find that the χ^2 value for the advection data is not as good as for the data when the initial dilution phase was ignored. So the early time fit to the concentration data is improved at the expense of the advection fit.

Table 5
Fitted values of entrainment coefficient and Froude number to the concentration and arrival time data. Fits allow for the initial dilution of the cylinder as described in the text

Slope	Entrainment coefficient	Frontal Froude number
All	0.016	0.80
0.04	0.009	1.03
0.086	0.018	0.69
0.1163	0.025	0.79

5.8. The experiments of Flacher et al. [5]

During the course of this study we became aware of experimantal ork undertaken recently ([5]) also investigating the motion of an instantaneously released cloud on uniform slopes. The work complements Schatzmann's, although at the time of writing no concentration measurements were available. Freon and argon were released instantaneously at differing aspect ratios and volumes on various slopes, including slopes identical to Schatzmann's. The scale of the releases was slightly larger than Schatz-

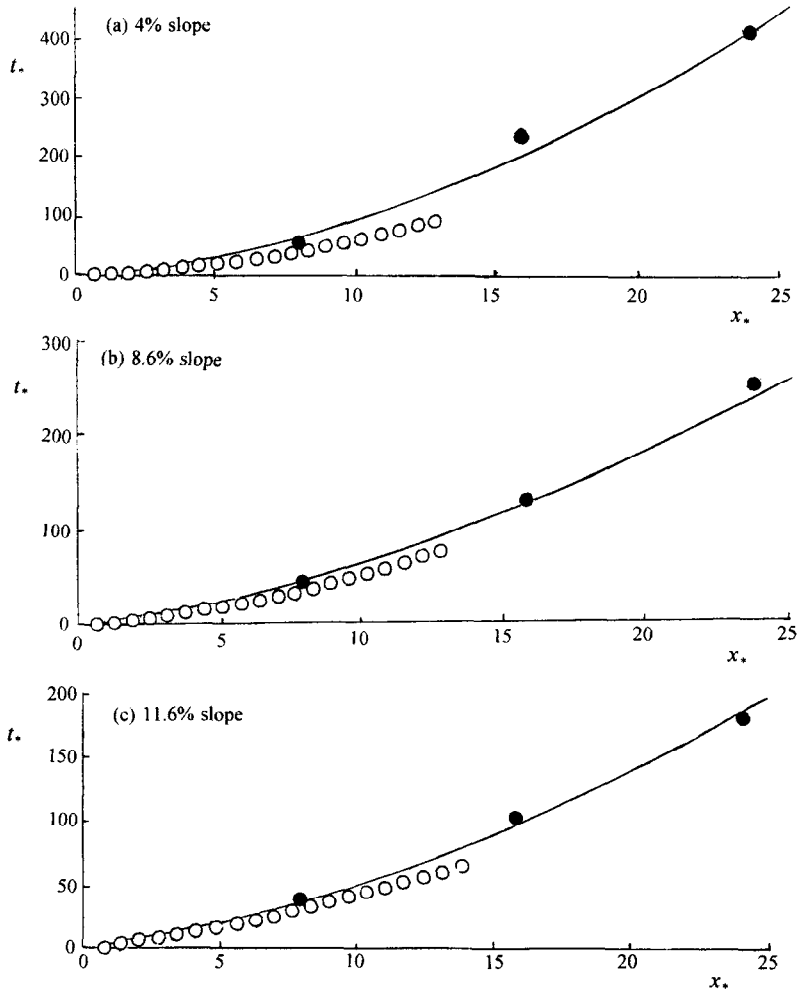

Fig. 5. (a)–(c) A comparison of the model with the measurements of Flacher et al. [5] (○) and Schatzmann et al. [4] (●) for three different slopes. The graphs are reproduced from Flacher et al. with the model predictions superimposed. The non-dimensionalisation is that of Flacher et al. $t_* = t/T$ and $x_* = X_f/L$ with $L = V_0^{1/3}$ and $T = (L/g_0')^{1/2}$.

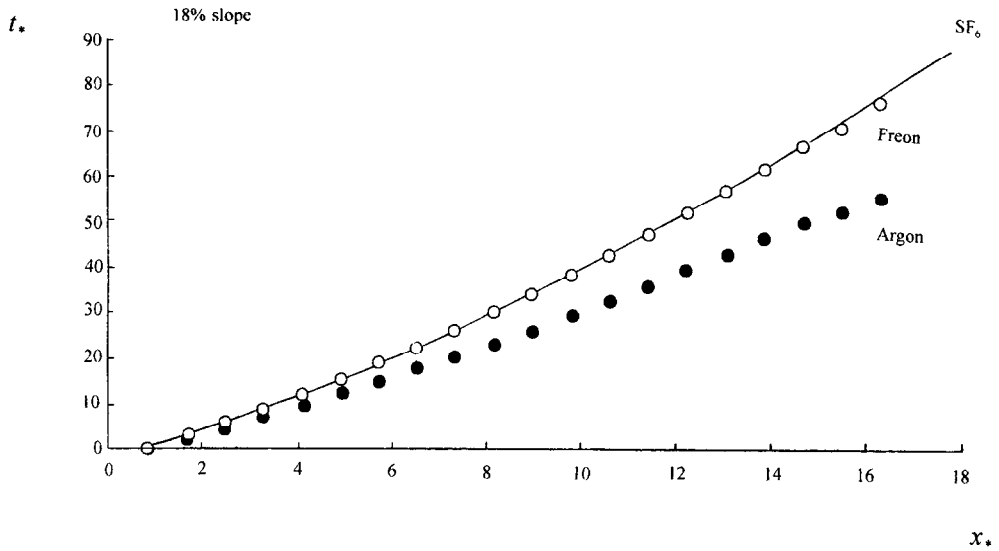

Fig. 6. A comparison of the model with the measurements of Flacher et al. [5] for releases of (○) Freon and (●) argon on a slope of gradient 18%. The graphs are reproduced from Flacher et al. with the model predictions superimposed. The non-dimensionalisation is that of Flacher et al. $t_* = t/T$ and $x_* = X_f/L$ with $L = V_0^{1/3}$ and $T = (L/g_0')^{1/2}$. The difference between the argon and Freon data may indicate an influence of the Reynolds number on the flow.

mann's, although generally measurements were at smaller non-dimensional distances and times. The position of the cloud front as a function of time was determined from video records.

Flacher's data, when put into non-dimensional form, appear to be generally consistent with Schatzmann's, although there does appear to be a slight tendency to higher (non-dimensional) advection velocities. The non-dimensionalisation in Fig. 5(a)–(c) and Fig. 6 is that of Flacher based upon $L = V_0^{1/3}$ and $T = L/g_0'$. Fig. 5(a)–(c) illustrates Flacher's data for Freon together with Schatzmann's and our model predictions (with slope independent entrainment coefficient and Froude number as determined from Schatzmann's data) for the three slopes studied here.

Also shown is our model prediction for an 18% slope compared with Flacher's data (Fig. 6). The agreement with Freon measurements appears to be remarkably good, given that we have not adjusted any coefficients for this slope (the entrainment coefficient and the Froude number have been given the values 0.034 and 0.59 respectively). The agreement may be fortunate given that a closer comparison of the shallower slopes indicates that the model with the above coefficients advects the cloud too slowly as compared with Flacher's data.

The failure of the argon data to collapse to the same curve in Fig. 6 is not understood. One possibility is that we should also consider ρ/ρ_a as a parameter, although we might expect this to have little effect once the cloud has diluted sufficiently. Flacher indicates that there may be some Reynolds number dependence by virtue of the higher viscosity

of argon, although like ρ/ρ_a we would expect this to have little effect once the cloud has diluted sufficiently.

6. Concluding remarks

We have shown how the wedge shaped cloud model of Webber et al. may be extended by the addition of an entrainment model. The main predictions of the entraining wedge model are that the concentration falls off with time as $t^{-3/2}$, and that the position of the cloud front varies as $t^{1/2}$. Experimental data appear to be broadly consistent with these predictions.

The model has two free parameters which need to be determined by experiment—the entrainment coefficient α_Γ and the frontal Froude number K_f. This is made more complicated by the fact that in principle both of these parameters may be slope dependent and that only limited data are available. This makes validation of the model against independent data almost impossible at present. Fitting these parameters to the data of Schatzmann indicates that good agreement for advection can be obtained by neglecting the slope dependence, but the concentration data seem to require that the product $\alpha_\Gamma K_f$ increases with slope Γ more rapidly than $\Gamma^{1/3}$. The entrainment coefficients obtained are small compared with 1 (typically around 0.03) and the Froude number appears to be around 0.6.

It also appears that initially the cloud dilution may be closer to that for a slumping cylinder. This is consistent with the spreading behaviour of one-dimensional shallow water model predictions ([3]), although of course these neglected dilution.

The conclusions of this study must remain tentative until there are more data with which to validate (or invalidate) the model. Good quality data of both the motion and the dilution of the cloud is required in order to validate this model.

Here we have only considered the case of zero ambient wind. We might consider adding terms which account for the wind; for example, it has been suggested that we might vectorially add the windspeed to the advection induced by the slope. But fundamental questions remain, as it is unlikely that when such influences are present the cloud will be able to maintain the wedge geometry that it might have in zero wind. Also, the model essentially considers only a balance of forces arising from resistance due to displaced air at the front of the cloud, whereas for very shallow slopes surface friction may come into play. These questions should be answered before one can have complete confidence in the application of such a model to hazard analysis.

Acknowledgements

Financial support for the work presented here has come from the STEP programme of the Commission of the European Communities, from the UK Health and Safety Executive, and from the Corporate Research programme of AEA Technology, all of which is gratefully acknowledged. The author thanks the following: Professor T. Fanneløp and his colleages at ETH Zurich for making experimental data available to us

before publication; Mr A. Mercer of the UK Health and Safety Executive for his useful comments on drafts of this manuscript; and Dr D.M. Webber of AEA Technology for much useful advice and guidance throughout the course of this work.

References

[1] D.M. Deaves and R.C. Hall, J. Loss Prevent. Process Ind., 3 (1990) 142.
[2] J. Nikmo and J. Kukkonen, Modelling Heavy Gas Cloud Advection in Complex Terrain, Finnish Meteorological Institute Preprint. (See also A model for the advection of a heavy gas cloud on a slope in Proc. Int. Conf. and Workshop on Modeling and Mitigating the Consequences of Accidental Releases of Hazardous Materials, ISBN 0-8169-0492-8, AIChE, 1991, p. 655).
[3] D.M. Webber, S.J. Jones and D. Martin, J. Hazard. Mater., 33 (1993) 101.
[4] M. Schatzmann, K. Marotzke and J. Donat, Research on continuous and instantaneous heavy gas clouds—contribution of sub-project EV4T-00210D to the final report of the joint CEC project, University of Hamburg, Meteorological Institute Report, 1990.
[5] A. Flacher, Diploma Thesis supervised by J. Müller and T.K. Fanneløp, Experimentelle Untersuchung der Ausbreitung einer Schwergaswolke auf geneigtem Grund, Institut für Fluiddynamik, ETH Zürich, 1994.
[6] P.W.M. Brighton, A.J. Prince and D.M. Webber, J. Hazard. Mater., 11 (1985) 155.
[7] B.R. Morton, G.I. Taylor and J.S. Turner, Proc. R. Soc. London, Ser A, 234 (1956) 1.
[8] T.H. Ellison and J.S. Turner, J. Fluid Mechanics, 6 (1959) 423.